

# Ultrasound Surface Extraction Using Radial Basis Functions

Rickard Englund and Timo Ropinski

Interactive Visualization Group, Linköping University, Sweden  
{rickard.englund,timo.ropinski}@liu.se

**Abstract.** Data acquired from ultrasound examinations is of interest not only for the physician, but also for the patient. While the physician uses the ultrasound data for diagnostic purposes the patient might be more interested in beautiful images in the case of prenatal imaging. Ultrasound data is noisy by nature and visually compelling 3D renderings are not always trivial to produce. This paper presents a technique which enables extraction of a smooth surface mesh from the ultrasound data by combining previous research in ultrasound processing with research in point cloud surface reconstruction. After filtering the ultrasound data using Variational Classification we extract a set of surface points. This set of points is then used to train an Adaptive Compactly Supported Radial Basis Functions system, a technique for surface reconstruction of noisy laser scan data. The resulting technique can be used to extract surfaces with adjustable smoothness and resolution and has been tested on various ultrasound datasets.

## 1 Introduction

Medical ultrasound imaging is modality of choice for various diagnostic examinations. Compared to other modalities ultrasound imaging has both benefits and drawbacks, for example it has a lower health risk than CT and MRI and ultrasound imaging is sometimes used as an alternative examination method [1], especially for pregnant patients [2]. Advancements in ultrasound imaging has allowed for data to be acquired at higher rates and higher resolution. This, in combination with more clinical evidence [3], has lead to more clinics using three and four dimensional ultrasound images as a tool to diagnosis.

Datasets acquired using ultrasound imaging differ from datasets acquired by other imaging methods such as CT and MRI in various ways. Voxel intensities of CT and MRI datasets represents the density at a certain location and we can classify samples by mapping ranges of densities to materials, such as bone and skin. In ultrasound images the voxel intensities represent the strength of the ultrasound echo which will have higher intensities at boundaries between regions and lower intensities in homogeneous regions. This sometimes makes it hard to apply visualization techniques developed for CT and MRI on ultrasound images without preprocessing. Furthermore, ultrasound images have a lower signal-to-noise ration than other techniques. Many filtering methods have been developed

for two dimensional ultrasound, while many of them can also be applied on the three dimensional data they do not always perform optimally. Speckle noise for instance, appears on two dimensions ultrasound images as a bright blob not connected to any tissue and can be ignored by the doctor while viewing the image. When rendering the data in three dimensions instead, speckle noise will become a opaque object and may occlude areas of interest.

Various filtering and rendering techniques have been presented to reduce the noise and allow for appealing renderings of ultrasound data [4–6]. These techniques mainly have clinical personnel as target group and often require high end computers to render with interactive frame rates. In this paper we explore the possibility to extract a smooth surface mesh from ultrasound data by first locating a set of surface points which are used to train a radial basis function system. The radial basis function system allows for smooth reconstruction of the surface and can be evaluated at any resolution which allows extraction a mesh at a desired resolution. By extracting a mesh we remove the requirement of volumetric data and it can be displayed on various devices and platform, even without hardware accelerated graphics processing units. Furthermore, the extraction of a smooth mesh allows for applying texture space rendering techniques used for realistic skin rendering in real-time applications and games [7–11].

## 2 Related Work

### 2.1 Ultrasound Visualization

There exists a lot of research targeting various stages of the ultrasound visualization pipeline, a detailed survey of the pipeline has been written by Birkeland et al. [12] where they present the current state-of-the-art research on the various stages.

Fattal and Lischinski [5] present a surface classification filter based on the Variational Principle resulting in a surface opacity volume. This filter will be further discussed in section 3. The opacity volume will contain non-zero voxels only on surfaces and they render this volume using oriented splatting. For each voxel with a value above a certain threshold they render a gradient oriented splat and setting its opacity to the voxel value which is then further modulated using a Gaussian falloff as the distance to the splats center increases.

Soltészová et al. [4] present a filtering technique using lowest-variance streamlines which successfully decrease the amount of speckle and random noise in the ultrasound data. For each voxel they try to find the streamline which has the lowest variance of voxel values. A number of samples is then taken along this streamline and the filtered voxel value is set to the mean of these samples.

### 2.2 Radial Basis Functions

Radial Basis Functions (RBF) have their origins in Artificial Neural Networks (ANN) and were first introduced by Broomhead and Lowe in their work in speech

recognition [13]. For a finite set of samples points  $x \in X$  with known values  $f \in \mathbb{R}$  they define an ANN as

$$S(x) = \sum_i^N \lambda_i \phi(\|x - x_i\|) \quad (1)$$

where  $\phi(r)$  is the basis function and  $\lambda_i$  is the, yet unknown, weight for kernel  $i$ . To find the weights  $\lambda$  such that the condition

$$S(x_i) = f_i \quad i = 1, 2, \dots, N \quad (2)$$

is fulfilled for all sample points  $x \in X$ , an inverse linear system has to be solved. A brute force solution of this linear system requires a memory usage of  $O(N^2)$  and a time complexity of  $O(N^3)$ . For smaller sets where  $N$  is rather small this is not a big issue but when  $N$  becomes large it becomes an issue.

Carr and Fright used RBFs to interpolate skull surfaces which is used to construct cranial implants [14]. By fitting a RBF to a depth-map obtained from ray-tracing CT data they manage to smoothly reconstruct a 3D-surface.

### 3 Surface Localization Using Variational Classification

The first step in our two stage algorithm is the surface localization, which applies the variational classification technique presented by Fattal and Lischinski [5]. For an input volume  $v$  they aim at finding a volume  $u$  which minimizes the function

$$F(v, u) = \alpha F_{iso} + \beta F_{tan} + \gamma F_{ind} \quad (3)$$

where  $\alpha$ ,  $\beta$  and  $\gamma$  are weights for the three parts  $F_{iso}$ ,  $F_{tan}$  and  $F_{ind}$ . Each of the three parts of  $F(v, u)$  allows  $u$  to have high values at certain features.  $F_{iso}$  is defined as

$$F_{iso} = \frac{u^2}{|\nabla v|^2 + \epsilon} (\omega |v - v_{iso}|^2 + (1 - \omega) |\tilde{v} - v_{iso}|^2) \quad (4)$$

which will make  $u$  tend towards zero everywhere except on boundaries of regions where  $v$  is close to the iso-value  $v_{iso}$ . To reduce the impact of noise the value from  $v$  will be blended with a value from a low-passed filtered volume  $\tilde{v}$  with blend factor  $\omega$ . The denominator  $|\nabla v|^2 + \epsilon$  is there to ensure uniform width along the boundaries. The second term,  $F_{tan}$  is defined as

$$F_{tan} = |\nabla u \times \nabla \tilde{v}|^2 \quad (5)$$

and will make the gradient of  $u$  tend to be as parallel as possible to the gradient of  $v$ . The final term,  $F_{ind}$  is defined as

$$F_{ind} = (\delta + (1 - \delta)|\nabla v|) (u - u_{ind}) \quad (6)$$

and is there to prevent a trivial solution ( $u = 0$ ) and to pull  $u$  towards the non-zero value  $u_{ind}$ . So far our  $u$  is unknown and since we want to find for which  $u$   $F(v, u)$  has a minimum we need to find the first derivative and where it evaluates to zero,

$$\frac{\delta F}{\delta u} - \frac{d}{dx} \frac{\delta F}{\delta u_x} - \frac{d}{dy} \frac{\delta F}{\delta u_y} - \frac{d}{dz} \frac{\delta F}{\delta u_z} = 0 \quad (7)$$

which will result in the following equation

$$\begin{aligned} u \left( \frac{\alpha (\omega |v - v_{iso}|^2 + (1 - \omega) |\tilde{v} - v_{iso}|)}{|\nabla v|^2 + \epsilon} \right) + \\ \beta (\nabla \times \nabla \tilde{v}) \cdot (\nabla u \times \nabla \tilde{v}) + \\ \gamma (\delta + (1 - \delta) |\nabla v|) (u - u_{ind}) = 0. \end{aligned} \quad (8)$$

Equation 8 can be written as a linear system  $Au = b$  where  $A$  is a sparse matrix and the vector  $b$  is defined by values from the volume  $v$  with one row for each voxel. Analytically we can get the volume  $u$  by first computing  $A^{-1}$  and then compute  $A^{-1}b$ , but this is a  $O(N^3)$  operation and since our  $N$  will be very large (number of voxels) it is not a practical solution. To solve the system we use the conjugate gradient solver in the C++ Eigen library.

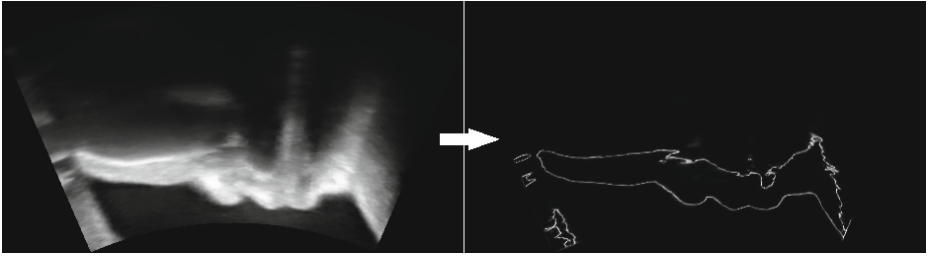


**Fig. 1.** Results of surface localization using variational classification

## 4 Surface Reconstruction with Radial Basis Functions

When the ultrasound data has been processed with the variational classification filter we have a volume consisting of only non-zero voxels close to surfaces, where a higher intensity means closer to the surface. From this surface volume we extract a point cloud where each voxel with a intensity above a certain threshold (a threshold of 0.2 has been used in all examples) becomes a point. In addition to the points position we also store the voxels surface intensity from the surface volume and the normalized gradient from the original ultrasound volume.

#### 4.1 Adaptive Compactly Supported RBFs

To create a mesh passing through the point cloud with a minimum error we use Adaptive Compactly Supported RBF, a technique presented by Ohtake et al. [15]. They define a function  $S(x)$  for a set of centers  $C = \{c_1, c_2, \dots, c_M\}$  as

$$S(x) = \sum_{c_i \in C} [g_i(x) + \lambda_i] \phi_{\sigma_i}(\|x - c_i\|) \quad (9)$$

where  $g_i(x)$  is a shape function for local approximation and  $\lambda_i$  is the RBF weights to minimize global error. The basis function  $\phi_{\sigma_i}(\|x - c_i\|)$  is the Wendland's compactly supported RBF [16] where  $\sigma_i$  is the support size of center  $c_i$  and  $\phi_{\sigma_i}(r) = \phi(r/\sigma_i)$  where

$$\phi(r) = \begin{cases} (1-r)^4(4r+1) & 0 \leq r \leq 1 \\ 0 & r > 1 \end{cases} \quad (10)$$

The centers are created iteratively such that all points  $x$  in the learning set  $X$  has an overlap above a certain threshold. In order to do this without creating to many centers Ohtake et al. defines two metrics, the first is a sample density  $d_i$  which are calculated over the  $K$  nearest neighbors as

$$d_i = c_i \sum_{j=1}^K \|x_i - x_j\|^2 \quad (11)$$

where  $c_i$  is the confidence of point  $x_i$ . The point cloud data that Ohtake et al. uses have an accuracy received from a laser scanner which is used as sample confidence, since we have volumetric data we treat the voxel value from the surface volume as confidence. The second metric is to measure the center overlap  $o_i$  at sample  $x_i$  and it is defined as

$$o_i = \sum_j \phi_{\sigma_j}(\|x_i - c_j\|). \quad (12)$$

The centers are created, one at a time, at the location of the sample point which currently has the lowest overlap. The creation of a center involves finding the optimal support size  $\sigma$  and the coefficients for the shape function  $g(x)$ . We want to find a support size  $\sigma$  such that it minimizes the local error

$$E_{local}(\sigma) = \left( \frac{1}{L} \sqrt{\frac{\sum_j d_j \phi_{\sigma}(\|x_j - c_i\|) \left( \frac{g_i(x_j)}{\|\nabla g_i(x_j)\|} \right)^2}{\sum_j d_j \phi_{\sigma}(\|x_j - c_i\|)}} \right)^2 + \frac{C}{\sigma^2} \quad (13)$$

where  $L$  is the length of the diagonal of a bounding box enclosing all sample points and  $C$  is calculated as

$$C = (T_{sa}L)^2 \quad (14)$$

where  $T_{sa}$  is a user defined constant controlling the smoothness of the reconstruction. The support size  $\sigma$  which gives the lowest local error is found by searching between a user defined upper and lower boundary. We evaluate the local error for a discrete set of support sizes within these boundaries starting with the minimum and step upwards until we find a support size where the local error is larger than the previous sample. In other words, we are stepping from the minimum and increasing the support size as long as the local error is decreasing. Once we find a point where the local error does not decrease we know that the optimal support size lies between this size and the size before that and we continue to search between these two sizes with a smaller step size. We search for local minimum until the difference between the two sizes are less than  $L \times 10^{-8}$ .

For each support size we need to fit a local shape function, which is defined as

$$g(x) = w - Au^2 - 2Buv - Cv^2 - Du - Ev - F \quad (15)$$

where  $u, v$  and  $w$  are the coordinates of point  $x$  transformed into the centers local orthonormal basis. The function  $g(x)$  is recognized as a quadratic surface and finding the coefficients  $A - F$  is a least-square problem where we want to minimize the error function

$$e = \sum_j d_j \phi_\sigma(\|x_j - c_i\|) g_i(x_j)^2 \quad (16)$$

which is a  $6 \times 6$  linear system. This system is trivial to solved using Eigen. When we have found the optimal support size and the corresponding shape function this center is complete and we continue with the next center. We continue to create new samples and update each samples overlap until each samples has at least an overlap above a certain threshold. Since only local points have been taken into consideration when fitting the local shape functions  $g_i(x)$  and centers overlap we still have a global error. Since we know that all sample points  $x_i$  are located on the surface this error can be calculated as the weighted average of the function  $S(x)$  as

$$E_{global}(\lambda) = \frac{1}{L} \sqrt{\frac{\sum_{j=1}^N d_j S(x_j)^2}{\sum_{j=1}^N d_j}}. \quad (17)$$

In order to fit the coefficients  $\lambda$  a minimizing problems is defined as

$$E_{reg}(\lambda) = E_{global}(\lambda)^2 + T_{reg} \|\lambda\|^2 \rightarrow \min \quad (18)$$

where  $T_{reg}$  is a positive real number and  $\|\lambda\|$  is defined as

$$\|\lambda\| = \sqrt{\frac{1}{M} \sum_i^M \left( \frac{\lambda_i}{\sigma_i} \right)^2}. \quad (19)$$

To find the minimum we need to find where the derivative of  $E_{reg}$  is zero which gives us the following system

$$\frac{\delta E_{reg}(\lambda)}{\delta \lambda} = 0 \Leftrightarrow (A + T_{reg}D)\lambda = b \quad (20)$$

where  $A$  is a sparse matrix of size  $M \times M$ ,  $D$  is a diagonal matrix and  $b$  is vector of size  $M$  where  $M$  is the amount of centers created in the local approximation. The entries in  $A$  is defined as

$$A_{ij} = \frac{\sum_k^N d_k \phi_{\sigma_i}(\|x_k - c_i\|) \phi_{\sigma_j}(\|x_k - c_j\|)}{L^2 \sum_k^N d_k}. \quad (21)$$

$A_{ij}$  will only be affected by points that is located in the intersection of the centers  $i$  and  $j$  since when a point  $x$  is outside one of the center the basis function  $\phi(r)$  will evaluate to zero. In other words row  $i$  in matrix  $A$  will only contain non-zero entries in columns  $j$  where centers  $c_i$  and  $c_j$  are overlapping. With a similar approach we define the values of  $b$ , where we iterate over all points  $x$  within center  $i$

$$b_i = \frac{\sum_k^N d_k \phi(\|x_k - c_i\|) (-S(x_k))}{L^2 \sum_k^N d_k}. \quad (22)$$

$S(x_k)$  can be interpreted as the error of the base approximation at point  $x_k$  since if  $S(x)$  where perfect it would return zero for any of the points in the points cloud. This means that the value of row  $b_i$  will be related to the current error of  $S(x)$ . The diagonal matrix  $D$  will have values based on the support size of current rows center

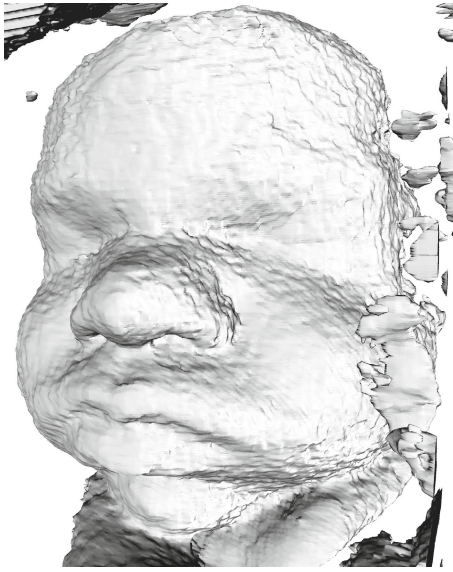
$$D_{ii} = \frac{1}{M} \left( \frac{1}{\sigma_i} \right)^2. \quad (23)$$

The sparse system in equation (20) is solved in a similar manner as the sparse system in Variational Classification described in section 3.

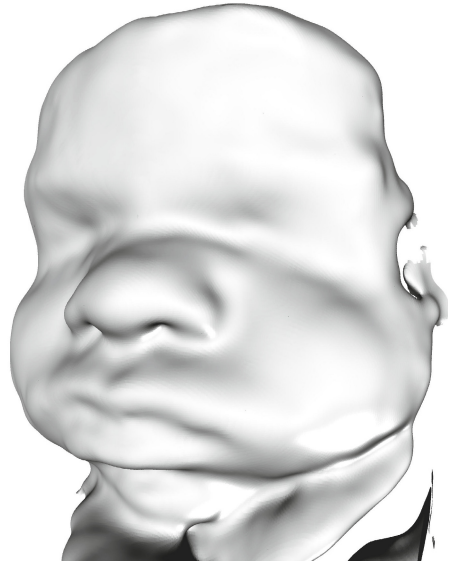
When the RBF weights have been fitted the only thing left is to extract the final mesh. By defining a regular grid enclosing the centers we can extract a mesh using the marching tetrahedron algorithm [17] and by allowing the user to vary the resolution of the regular grid meshes can be extracted at desired resolution. In order to save computational power we only evaluate on grid cells which are close enough to a center to contribute to the surface.

## 5 Results and Discussions

The described techniques have been successfully tested on various ultrasound dataset. In figure 1 we see one slice of before and after the variational classification has been applied on an ultrasound dataset ( $467 \times 255 \times 101$ ). The variational classification took 5.172 seconds to complete, including building and solving the



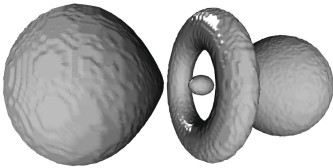
(a) Marching tetrahedron



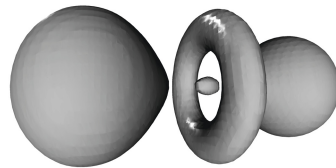
(b) Radial Basis Functions

**Fig. 2.** Comparison between a surface extracted from a fetus ultrasound dataset with marching tetrahedron and our approach

linear system resulting in 189,362 significant voxels. These voxels is then used as a point cloud to train the Adaptive Compactly Supported RBFs system as described in section 4.1 and the result from that is shown in figure 5b. Of the 189,362 input samples 2536 centers is created. The surface that has been extracted using our approach is smoother then the noisy surface extracted with marching tetrahedron, which is clearly visible in figure 5 where both surfaces has been extracted with same iso-value and same resolution.



(a) Marching tetrahedron



(b) Radial Basis Functions

**Fig. 3.** Comparison between a surface extracted from a simulation dataset of a hydrogen atom with marching tetrahedron and our approach



The presented technique has been developed with ultrasound as main modality, though, it can also be applied to other types volumetric dataset. For example we have used a simulated dataset of hydrogen wavefunction for verification purposes. Iso-surfaces of the hydrogen wavefunction is smooth by nature and a surface extracted using our approach look similar to a surface extracted using the original data which can be seen in figure 5.

## 6 Conclusions

We have presented a technique that bridges research in ultrasound data processing with research in surface reconstruction of noisy point cloud data. By localizing surface voxels in a 3D ultrasound dataset and represent them as a point cloud we can utilize results obtained in surface reconstruction from laser scan data. Our results show that combining these two fields is promising, as not only both fields do handle data with some degree of noise, but they are both relying on the acquisition of a reflected signal using a sender/receiver system.

While the presented techniques only handles smooth reconstruction of the surfaces we do not currently handle any speckle or random noise. In future research it would be interesting to include other filtering techniques such as the lowest-variance streamlines filtering [4] for speckle removal.

All 3D renderings in this paper use Phong illumination to shade the surfaces. It would be interesting to extend our rendering or export the mesh into another system to make use of available advance skin rendering techniques [7–11].

**Acknowledgements.** The authors would like to thank Isabelle W Hachette at ContextVision AB, Linköping Sweden, for supplying the ultrasound test data used in this project.

## References

1. Levine, D.: Use of ultrasound as an alternative to ct (2010)
2. Coakley, F.V., Cody, D.D., Mahesh, M.: The pregnant patient: Alternatives to ct and dose-saving modifications to ct technique. *Image Wisely* (November 2010)
3. Wegmann Hachette, I.: 3d/4d ultrasound imaging: Coming of age (2013)
4. Šoltészová, V., Helljesen, L.E.S., Wein, W., Gilja, O.H., Viola, I.: Lowest-variance streamlines for filtering of 3d ultrasound. In: *Eurographics Workshop on Visual Computing for Biology and Medicine (VCBM 2012)*, pp. 41–48 (2012)
5. Fattal, R., Lischinski, D.: Variational classification for visualization of 3d ultrasound data. In: *Proceedings of Visualization, VIS 2001*, pp. 403–410. IEEE (2001)
6. Farzana, E., Tanzid, M., Mohsin, K.M., Bhuiyan, M.I.H., Hossain, S.: Adaptive bilateral filtering for despeckling of medical ultrasound images. In: *TENCON 2010-2010 IEEE Region 10 Conference*, pp. 1728–1733. IEEE (2010)
7. d’Eon, E., Luebke, D., Enderton, E.: Efficient rendering of human skin. In: *Eurographics Symposium on Rendering* (2007)

8. Jensen, H.W., Marschner, S.R., Levoy, M., Hanrahan, P.: A practical model for subsurface light transport. In: Proceedings of the 28th Annual Conference on Computer Graphics and Interactive Techniques, pp. 511–518 (2001)
9. Mikkelsen, M.S.: Skin rendering by pseudo-separable cross bilateral filtering. Naughty Dog Inc. (2010)
10. Jimenez, J., Whelan, D., Sundstedt, V., Gutierrez, D.: Real-time realistic skin translucency. IEEE Computer Graphics and Applications 30, 32–41 (2010)
11. Debevec, P.: Digital ira (2012)
12. Birkeland, Å., Solteszova, V., Hönigmann, D., Gilja, O.H., Brekke, S., Ropinski, T., Viola, I.: The ultrasound visualization pipeline-a survey. arXiv preprint arXiv:1206.3975 (2012)
13. Broomhead, D.S., Lowe, D.: Radial basis functions, multi-variable functional interpolation and adaptive networks. Technical report, DTIC Document (1988)
14. Carr, J.C., Fright, W., Beatson, R.K.: Surface interpolation with radial basis functions for medical imaging. IEEE Transactions on Medical Imaging 16, 96–107 (1997)
15. Ohtake, Y., Belyaev, A., Seidel, H.-P.: 3d scattered data approximation with adaptive compactly supported radial basis functions. In: Proceedings of Shape Modeling Applications, pp. 31–39. IEEE (2004)
16. Wendland, H.: Piecewise polynomial, positive definite and compactly supported radial functions of minimal degree. Advances in Computational Mathematics 4, 389–396 (1995)
17. Treece, G.M., Prager, R.W., Gee, A.H.: Regularised marching tetrahedra: improved iso-surface extraction. Computers & Graphics 23(4), 583–598 (1999)

## Appendix: Parameters

**Table 1.** Parameters used in the Variational Classification

Parameter	Value
$\alpha$	0.6
$\beta$	0.03
$\gamma$	0.1
$v_{iso}$	0.6
$\omega$	0.1
$\xi$	0.5
$u_{ind}$	1.0

**Table 2.** Parameters used in the Adaptive Compactly Supported RBF

Parameter	Value
$K$	20
Min Overlap	1.6
Support size boundaries	[0.001 0.3]
$T_{sa}$	$10^{-5}$
$T_{reg}$	$10^{-6}$
Mesh resolution (longest axis)	450